

# Texture and strain analysis of the ferroelastic behavior of $\text{Pb}(\text{Zr,Ti})\text{O}_3$ by *in situ* neutron diffraction

Robert C. Rogan, Ersan Üstündag,<sup>a)</sup> and Bjørn Clausen

Department of Materials Science, California Institute of Technology, Pasadena, California 91125

Mark R. Daymond

ISIS Neutron Scattering Facility, Rutherford-Appleton Laboratory, Chilton, Didcot, OX110QX, United Kingdom

(Received 9 August 2002; accepted 16 January 2003)

*In situ* uniaxial compression experiments on  $\text{Pb}(\text{Zr,Ti})\text{O}_3$  or PZT-based polycrystalline electroceramics were conducted using time-of-flight neutron diffraction. Elastic lattice strain and texture evolution were observed in PZT's near the edge of the morphotropic phase boundary (with tetragonal and rhombohedral phases present). Multiphase Rietveld analysis yielded anisotropic lattice strain evolution curves in directions parallel and perpendicular to the loading axis for both phases. A quantitative analysis of the domain switching under applied stress was possible through application of a March–Dollase model for texture. © 2003 American Institute of Physics.  
[DOI: 10.1063/1.1558229]

## I. INTRODUCTION

Ferroelectric ceramics are widely used in a diverse set of devices including sensors, actuators, transducers, and ultrasonic motors. In these applications, they exhibit a complicated coupled behavior in response to both electrical and mechanical loading and often experience internal stresses which lead to significant fatigue and eventually failure.<sup>1</sup> Efforts to model and predict the behavior of ferroelectrics have often been hindered by the lack of suitable constitutive relations that accurately describe the electromechanical response of these materials. Recently, self-consistent models have been developed to describe the behavior of polycrystalline ferroelectrics.<sup>2</sup> These models are essentially an adaptation of the self-consistent crystal plasticity scheme developed by Hill and Hutchinson and are able to capture some important features of ferroelectric behavior such as electromechanical hysteresis. The formulation of robust models for ferroelectric materials requires knowledge of their crystallographic behavior under applied mechanical and electrical loading. Specifically, it is desirable to obtain, as a function of applied electromechanical loads, quantitative data of the microscopic strain states which are functions both of single crystal elastic properties and domain switching and/or pinning.

Many investigations of PZT's (and other ferroelastic and ferroelectric materials) have been undertaken to study the macroscopic stress-strain response via traditional mechanical testing,<sup>1–4</sup> as well as crystal structure and orientation analysis using x rays<sup>5–11</sup> and neutrons.<sup>12–18</sup> While macroscopic measurements have been invaluable for outlining the behavior of multiphase materials and isolating industrially useful compositions, they offer no insight into the crystallographic behavior which is valuable to the modeling community. X-ray studies have been particularly useful in ascertaining crystal structure and observing the texture effects of domain

switching, both *in situ* and *ex situ*. However, the large majority of these studies are hindered by the limitations of x-ray penetration depths in a material in which the element lead contributes approximately 60% of the density. For instance, most x-ray studies employed  $\text{Cu } K\alpha$  radiation which has less than 5  $\mu\text{m}$  penetration into PZT.

Neutron diffraction is an ideal probe of bulk crystallographic structure, but so far studies have mostly concentrated on probing the temperature–composition–structure relationship to obtain a clear understanding of the nature of the various phase transitions. A neutron diffraction study<sup>17</sup> is noted as it investigated the ferroelastic behavior of a single crystal  $\text{LaNbO}_4$  under compressive stress. Although this study did provide valuable insight about the crystallographic domain switching mechanism in  $\text{LaNbO}_4$ , it did not involve a polycrystalline material and, therefore, could not probe the interactions between various domains and grains. We report an *in situ* bulk crystallographic study of the ferroelastic behavior of a multiphase, polycrystalline PZT under compressive loading. Simultaneous extraction of the lattice strains and quantitative texture effects (domain switching) was possible through a careful whole-pattern Rietveld analysis.

## II. EXPERIMENTAL PROCEDURE

### A. Sample description

Several  $\text{Pb}(\text{Zr,Ti})\text{O}_3$  (PZT) specimens were obtained from American Piezo Ceramics, Inc. (Mackeyville, PA 17750). Samples were cylindrical and measured approximately 6.35 mm in diameter by 16 mm in length. Each specimen was prepoled by the manufacturer in an electric field of 2.5 kV/mm (applied along the axial direction). This field is well beyond the coercive field of this material and induced the expected remnant polarization. Chemical composition was determined with an electron probe analyzer (Jeol JXA-733 SEM equipped with wavelength-dispersive spectrometers). Average quantitative atomic fractions were found

<sup>a)</sup> Author to whom correspondence should be addressed; electronic mail: Ersan@caltech.edu

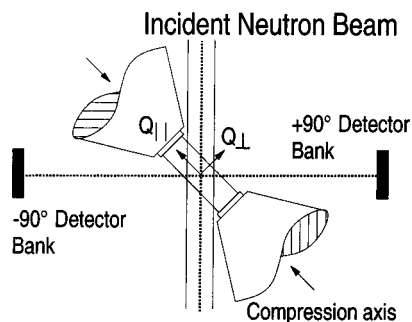


FIG. 1. Sample-detector geometry at ENGIN allowing for simultaneous measurement of longitudinal and transverse sample behavior by the  $2\theta = -90^\circ$  and  $2\theta = +90^\circ$  detectors, respectively.

based on measurements taken at seven random, spatially isolated sample locations. The Zr/Ti atomic ratio was measured to be approximately 49/51 (disregarding small amounts of dopants such as Sr, Ba and Sb, each  $\leq 2$  at. %). At room temperature, this composition places the sample in the traditional morphotropic region of the phase diagram.<sup>19</sup> As will be shown later, it was indeed found that both the tetragonal and rhombohedral phases were present in the specimens.

## B. Neutron diffraction experiments

A powder sample of the PZT was obtained by crushing some cylinders using a mortar and pestle. A time-of-flight (TOF) neutron diffraction pattern of this powder was collected using the SMARTS diffractometer<sup>20</sup> at the Los Alamos Neutron Science Center. The powder was placed in a vanadium can and data were collected for approximately 12 h. All subsequent experiments were conducted at the Rutherford Appleton Laboratory's ISIS Facility in the ENGIN diffractometer. Here, *in situ* TOF neutron diffraction patterns of prepoled solid PZT samples were obtained at various uniaxial compressive loads (see Ref. 21 about the description of the loading setup at ENGIN). Observation of both the axial and transverse strains was possible due to the sample orientation and the detector geometry (Fig. 1). Strain gauges attached to the samples measured macroscopic axial strain during diffraction experiments. Data acquisition times were approximately 1 h at each load level. Small transient relaxation effects were noted following each load change (a maximum of 0.015% strain over 15 minutes before stabilization), but these effects were deemed negligible for the purposes of this study.

## III. DIFFRACTION DATA ANALYSIS

### A. Powder specimen

Neutron spectra were analyzed by the Rietveld method<sup>22</sup> using the GSAS software package.<sup>23</sup> cursory preliminary analysis of the data collected from both diffractometers indicated that this material was most likely a two-phase system, as evidenced by the presence of intensity between tetragonal peak doublets.<sup>5,6,12,13</sup> The signal-to-noise ratio of the data collected at ISIS was insufficient (due to short collection times) to perform any detailed, reliable dual-phase crystallographic analysis. Instead, data from the SMARTS diffracto-

meter were selected for detailed analysis because of the lengthy acquisition time. Crystallographic data obtained from previous studies on PZT's were employed as a starting point in the analyses.<sup>5,13</sup> In particular, space groups  $P4mm$  and  $R3m$  were used for the tetragonal and rhombohedral phases, respectively. The  $R3m$  model was instituted using the symmetry operators of the  $R3c$  space group while constraining the oxygen atomic positions so that  $2O_y = O_x$  and  $O_z = 1/12$ .<sup>5,14</sup> These impositions were used to define and relate the origin of the two space groups.

The average atomic occupancies were determined from the electron microprobe analysis and were initially assumed to be the same for both phases. Atomic positions and isotropic thermal parameters were constrained to be the same for chemically identical sites; i.e., dopant atoms were required to mimic the atoms they replaced. This did not apply for the Zr and Ti positions and thermal parameters, which were allowed to refine independently. The background function was modeled using a ten term power series (TOF function No. 6),<sup>23</sup> which is the regular function for the SMARTS diffractometer. A Von Dreele–Jorgensen–Windsor convolution function (TOF function No. 1) (Ref. 23) was used for the peak profiles of each phase. The peak widths for both phases were refined independently.

Convergent values for refinement parameters such as the histogram scaling factor, lattice parameters, peak widths, phase fractions, background coefficients, and linear absorption coefficient were initially determined. This was followed by refinement of the independent isotropic thermal parameters and atomic positions. All atomic positions were refined except for the Pb position in the tetragonal phase (to preserve the origin of the space group), and the oxygen positions for the rhombohedral phase were constrained as mentioned above. Refined individually, none of the atomic site occupancies offered significant deviations from the average calculated chemistry. Considering the short collection times for the ENGIN spectrometer data, even moderate ( $\sim 5\%$  per site) changes in atomic occupancies were not observed to have a significant impact on the overall quality of the refinements. The powder diffraction analysis could not therefore provide any compelling evidence for altering the stoichiometric data from the microprobe analysis in order to achieve better fits for the compression loading spectra.

Some of the problems generally associated with Rietveld refinements of PZT's were also noted in this analysis.<sup>5,12–14</sup> For instance, the isotropic thermal parameters of the Zr and Ti atoms were slightly different despite occupying the same crystallographic site in the tetragonal phase. The introduction of anisotropic thermal parameters induced significant instabilities due to the complexity of the background, and they were subsequently removed from the model. The literature, too, exhibits significant scatter in various crystallographic parameters. Since the purpose of the present study was not to perform a detailed crystallographic analysis of this PZT composition, but to systematically investigate the effects of mechanical loading on the material, the current analysis was considered satisfactory. For possible explanations of these behaviors, the reader is referred to studies investigating similar issues.<sup>5,12–16,24,25</sup>

Final refinements of the powder specimen produced a weighted residual  $R_{wp}=1.7\%$ ,<sup>26</sup> indicating a good match between the Rietveld model and experimental data despite some problems fitting a complicated low- $d$ -spacing background present in the SMARTS data set.<sup>22,23,26</sup> Lattice parameters were  $a_T \approx 4.0482$  Å and  $c_T \approx 4.116$  Å for the tetragonal phase, while for the rhombohedral phase  $a_R \approx 5.765$  Å and  $c_R \approx 14.193$  Å. These parameters are in good agreement with previous studies using similar models.<sup>5,13,14</sup> The peak widths of the two phases were found to differ by only 7% and were thus considered to be the same in further analysis.<sup>5</sup> The Rietveld refinement yielded final volumetric phase fractions of roughly 79% tetragonal and 21% rhombohedral. These numbers confirm that the material is indeed in the morphotropic region of the phase diagram in agreement with the Zr/Ti ratio measured by the electron microprobe analysis. Comprising approximately one-fifth of the sample volume the rhombohedral phase is expected to affect the macroscopic properties of this material. It is important to note, however, that due to the large size of the rhombohedral phase's unit cell, its fractional contribution to the diffracted intensity is much less than its volumetric phase fraction.

## B. Loaded specimen

Crystallographic data obtained from the SMARTS powder pattern was implemented in the ENGIN data analysis. None of the atomic positions or thermal parameters were refined for this data set. Any attempts to do so resulted in divergence during the least-squares calculation. For the ENGIN data, a six-term power series was used for the background (TOF function No. 6) (Ref. 23) and a back-to-back pseudo Voigt function for the peak profiles (TOF function No. 3) (Ref. 23). The peak widths of the two phases were constrained to be the same,<sup>5</sup> an assumption which was validated by the analysis of the powder as described above. For each detector bank, the zero-load pattern refinement provided the linear absorption coefficient for the model, which was then held fixed for all higher-load levels. Absorption values were on the order of 4% for each bank. Patterns for each load level were refined using flags for the lattice parameters, peak widths, histogram scale factor, texture variables, and background coefficients.

Contrary to the powder, the poled sample displayed significant texture effects in the diffraction pattern. It is well known that PZT exhibits polarizations aligned along the [001] direction of the tetragonal phase and the [111] axis in the pseudocubic unit cell of the rhombohedral phase, and that the diffracted intensities from related reflections can be used to measure extent of domain alignment in these materials.<sup>5,7–10</sup> Due to the sample-detector geometry, crystalline texture in the specimen could be modeled in a simple manner. The March–Dollase function in GSAS is aptly suited to account for the effects of texture on diffracted intensity for cylindrical samples:<sup>27–29</sup>

$$I_{hkl} \propto P_{hkl}(\alpha) F_{hkl}^2, \quad (1)$$

$$P_{hkl}(\alpha) = [r^2 \cos^2(\alpha) + r^{-1} \sin^2(\alpha)]^{-3/2}. \quad (2)$$

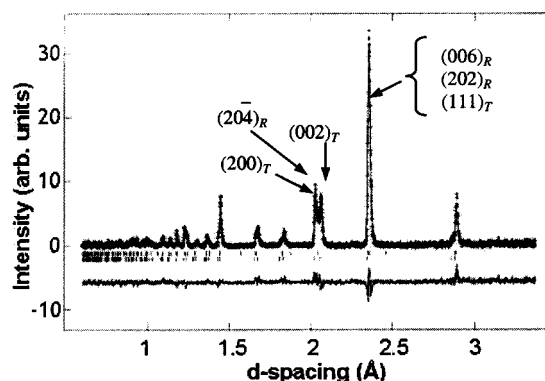


FIG. 2. A typical neutron diffraction pattern obtained at zero load in the longitudinal direction. The experimental data are shown as crosses fitted by the Rietveld model. The bottom curve designates the difference between the two. The upper tick marks show the positions of rhombohedral ( $R$ ) peaks while the lower ones indicate those for the tetragonal ( $T$ ) phase. Some important reflections for each phase are marked. The high intensity of the  $(002)_T$  reflection suggests a high degree of domain alignment along the longitudinal (or axial) direction as would be expected from the electrical poling.

Here  $I_{hkl}$  is the intensity of a given diffraction peak,  $F_{hkl}^2$  is the structure factor, and  $P_{hkl}$  is the March function. This function is a true distribution function and describes the density of poles at a given angle ( $0 \leq \alpha \leq \pi/2$ ). Only the March coefficient  $r$  needs to be defined to yield a complete description of the texture in the sample. In other words, the entire orientation distribution function can be described in this special case of fiber texture in a cylindrical sample. It is also a very flexible model in that it is applicable to distributions which have a maximum at  $\alpha=0$  ( $r<1$ ) or a maximum at  $\alpha=\pi/2$  ( $r>1$ ).

Applying the March–Dollase model to the tetragonal phase was straightforward: the [001] direction corresponds to the crystallographic dipole, and the angle between domains discernable in a diffraction experiment is  $90^\circ$ , so texture in this phase could be modeled easily by tracking the intensity variations between the prominent (200)–(002) doublet (Fig. 2).<sup>5,9,10,30</sup> Using a preferred orientation axis of [001] in GSAS and refining the March coefficient for this family of peaks significantly reduced the  $R_{wp}$  values for all fits.

The rhombohedral phase, however, was slightly more complicated. The dipole formed due to ion displacement along the [111] direction in the pseudocubic unit cell corresponds to the [006] direction in the  $R3c$  structure.<sup>14</sup> In this phase, domains form at either  $71^\circ$  or  $109^\circ$ , reflecting a dipole realignment in one of the [11-1] directions of the pseudocubic cell geometry or the [202] directions of the  $R3c$  space group.<sup>5,9,10,30</sup> For this reason, this study investigated the  $R3c$  (006) and (202) reflections. Unfortunately, both of these reflections lie in the region of the high-intensity (111) peak of the tetragonal phase centered at roughly  $2.35$  Å in the diffraction patterns (Fig. 2). The convolution of intensities therefore produces a large and relatively broad single peak. Unambiguous assignment of relative intensities in this region using single-peak fits was not possible due to the destabilizing effects of the instrumental peak width and the relatively low signal-to-noise ratio resulting from short collection times

at ENGIn. The constraints imposed on lattice parameters during whole-pattern Rietveld refinements countered these effects by strictly limiting the uncertainty in the peak positions. Using a preferred orientation axis of [006] and refining the March coefficient for this peak and its equivalents improved all fits. Still, the (006)–(202) region of the fitted spectra consistently displayed fitting errors greater than the rest of the pattern which indicate that the crystal model does not sufficiently account for the observed intensity.

The superfluous observed intensity (see Fig. 2) likely represents texture effects due to the (202) peak of the rhombohedral phase. Since the angle between the [202] and [006] directions is the angle between  $71^\circ$  or  $109^\circ$  domains (which are therefore not orthogonal), following the texture in only one preferred orientation axis does not sufficiently account for the intensity changes in the other peak. Attempts to correct this error by introducing a second preferred orientation axis (the [202]) were met with mixed success. Since this is a secondary texture effect in a minority phase, GSAS treated the (202) March coefficient as a free variable, which destabilized fits. While individual patterns' residuals were improved, the resulting values for texture and lattice parameters were unreasonable, and the refinements of some spectra failed to converge. It was concluded that the current data would not support resolution of this quantity, so the [202] preferred orientation axis was removed from the model.

The final discrepancies between the calculated neutron spectrum for the loaded sample and the measured diffraction data as quantified by the weighted residual  $R_{wp}$  were around 18% for the longitudinal detector data and 19% for the transverse. While these residuals are generally considered high by Rietveld standards, they are a reflection of the effects of the signal-to-noise ratio, rather than indications of gross miscalculation ( $\chi^2$  values were approximately 1 for both banks).<sup>26</sup> The slightly higher values for the transverse bank are due to the fact that it samples only a limited angular space of the  $2\pi$  specimen circumference (roughly 4%), while the longitudinal bank samples the entire polar angle range from 0 to  $\pi$  with respect to the sample's cylindrical axis.

## IV. RESULTS AND DISCUSSION

### A. Macroscopic deformation

Figure 3 displays the results for the longitudinal (axial) macroscopic sample strain as measured by the strain gauge during the loading procedure. Strains are referenced from the poled (zero-load) configuration, ignoring any residual strains induced by the pressing, sintering, or poling processes. It is seen that the initial elastic region is very small, below  $-25$  MPa. Notice the large changes in strain during the stress changes between  $-25$  and  $-100$  MPa. This range corresponds to that of  $90^\circ$  domain switching in the tetragonal phase and  $71^\circ$  and  $109^\circ$  domain switching in the rhombohedral phase previously noted in PZT materials.<sup>5,9,10,30</sup> Upon reaching  $-150$  MPa, the switching process has saturated and the sample's initial polarization along its cylindrical axis will have largely vanished. This is in effect the mechanical "depoling" of an electrically poled PZT. At stresses greater than  $-150$  MPa, the material again exhibits nearly linear elastic

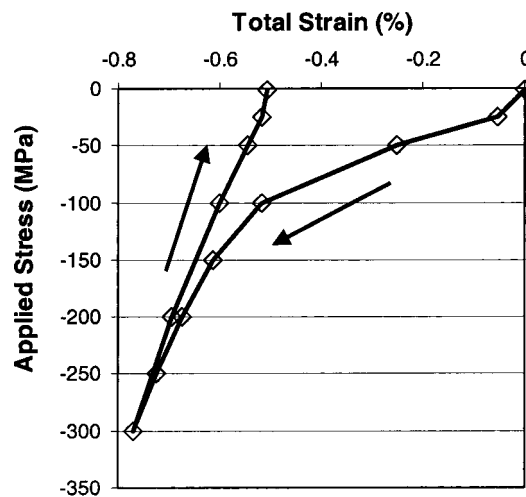


FIG. 3. Axial (longitudinal) macroscopic sample strain as measured by a strain gauge during the loading cycle. The diamonds indicate the locations where neutron data were collected. Note that the reference point for strain was taken to be the zero load position.

behavior. During unloading, most of the domains apparently remain in their switched position, an effect of the well-known electromechanical hysteresis exhibited by these materials. This results in a large residual strain in the longitudinal direction upon unloading. Texture and lattice strain evolution data obtained from neutron diffraction support these observations.

### B. Tetragonal phase

The texture observed in the specimen changed significantly over the course of loading and unloading due to domain switching. Figure 4 shows the changes in the March coefficient of the tetragonal phase ( $r_T$ ) as a function of applied stress. The value of  $r_T$  is initially less than 1.0 as seen in the longitudinal bank [Fig. 4(a), diffraction vector parallel to sample axis], representative of a large number of crystallographic [001] poles aligned with the sample's cylindrical axis. This is expected since the sample was prepoled in this direction, implying that microscopic dipoles of individual domains should align with the poling field. As the load is increased,  $r_T$  quickly passes through the random powder texture value of 1.0 and proceeds to increase dramatically up to a value of about 1.4 between  $-100$  and  $-150$  MPa applied stress. Since  $r_T$  values greater than 1.0 correspond to a distribution function with a maximum at  $\alpha = \pi/2$ , the diffracted intensities detected in the longitudinal bank above  $-150$  MPa are indicative of a majority of [001] poles aligned along a direction normal to the sample axis (the transverse direction). This increase is a direct observation of the  $90^\circ$  domain switching in the tetragonal phase, consistent with the switching of domains that initially were oriented with their  $c$  axis parallel to the loading direction reorienting such that the  $c$  axis becomes perpendicular to the loading axis. Above  $-150$  MPa, the switching process has saturated, and the  $r_T$  value is roughly constant. During the unloading procedure, most of the switched domains remain locked and cannot return to their original configuration, as indicated by

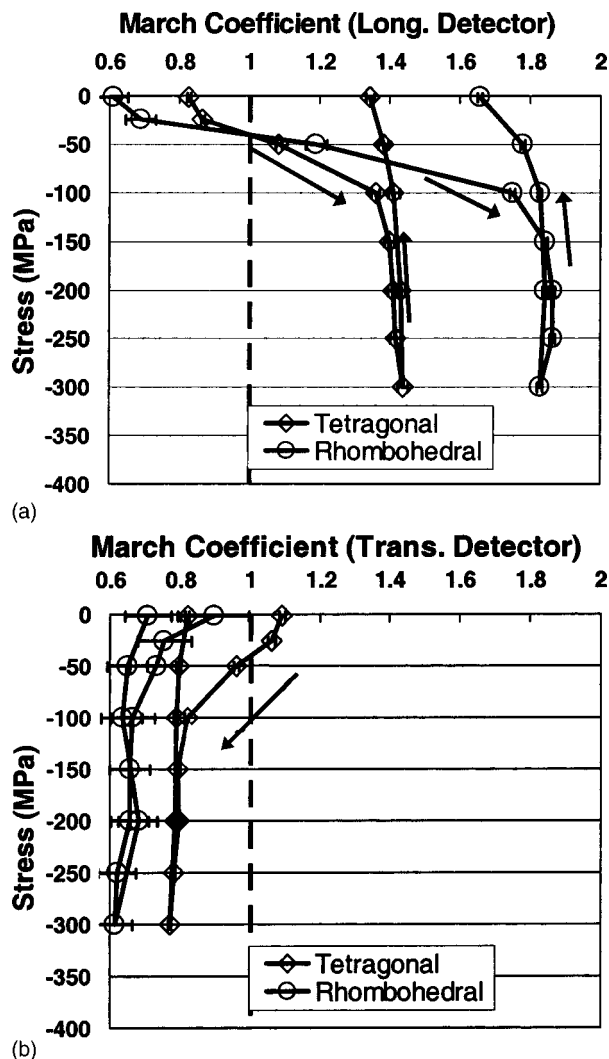


FIG. 4. March coefficients measured in the longitudinal (a) and transverse (b) detectors as a function of applied stress. Arrows indicate direction of load changes.

the roughly constant value of the March coefficient. Only a slight decrease is noted between  $-50$  MPa and  $0$  MPa, corresponding to the relaxation of a small fraction of domains.

The transverse detector bank [Fig. 4(b)] is oriented such that the relevant diffraction vector is  $90^\circ$  from the sample axis. At this position, it is seen that  $r_T$  is initially greater than  $1.0$  at zero load and decreases to a value less than  $1.0$  during the course of loading. This means that the transverse bank corroborates the data from the longitudinal bank: it observes the majority of  $[001]$  poles initially aligned with the sample axis and, after the switching procedure, observes a majority aligned in the direction normal to the sample axis. The difference in the magnitudes of the March coefficients observed between the two banks is probably due to the limited sampling range of the transverse bank. When domains switch from their initial position, they may move into any of the energetically equivalent  $90^\circ$  orientations normal to the sample axis. In other words, after switching the poles are distributed around the  $2\pi$  solid angle of the cylinder, but the transverse detector only measures texture from poles aligned in a  $4\%$  fraction of this circumference.

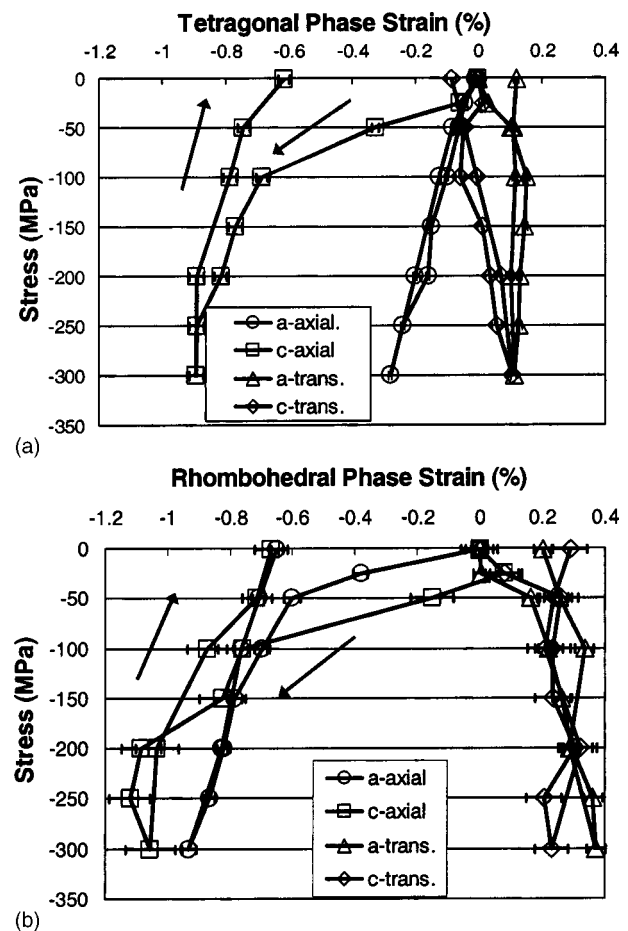


FIG. 5. Lattice strain in the tetragonal (a) and rhombohedral (b) phases as a function of applied stress. The "axial" data were derived from diffraction patterns collected at the longitudinal detector while the "trans." data were obtained from the transverse detector. Arrows indicate direction of load change.

The description of the switching process given above helps with the interpretation of the lattice strains measured in the tetragonal phase [Fig. 5(a)]. Here the labels "axial" and "trans." refer to the macroscopic sample directions of the cylindrical axis and the direction perpendicular to it, respectively. All measurements are referenced to the poled sample configuration (the zero-load state), ignoring any lattice strains induced by the pressing, sintering, or poling processes. Error bars are those reported by GSAS after convergence and are representative only of fitting errors. One must remember that each detector only measures the spacing between certain crystal planes which fulfill the diffraction condition. At this point, it will help to consider the evolution of a single, initially poled tetragonal domain throughout the loading procedure. In the zero load configuration, this hypothetical domain is oriented such that its  $c$  axis is parallel to the loading axis and the associated planes satisfy Bragg's law with respect to the longitudinal detector. The planes along the  $a$  axis in this domain do not. Therefore, only information on the  $c$  axis is available to the longitudinal detector and no intensity is present from the  $a$  axis. At some applied load, internal stresses will force this domain to reorient itself, switching  $90^\circ$ . Now the domain's  $a$  axis planes fulfill the

diffraction condition and contribute intensity to the pattern in the longitudinal detector; correspondingly the  $c$  axis information has effectively disappeared from the spectra. In terms of the time-of-flight diffraction peaks, this change is manifested during the course of compressive loading by the disappearance of intensity for the  $(002)_T$  peak and appearance of intensity in the  $(200)_T$  peak. In the transverse detector, the opposite behavior has been recorded: as the domains switch to reorient their  $c$  axis in the transverse direction, the intensity in the  $(002)_T$  peak is introduced and intensity in the  $(200)_T$  peak is lost. In a polycrystalline sample with many domains these effects occur in a continuous manner.

Returning now to the lattice strain evolution, Fig. 5(a) shows that for domains oriented with their  $c$  axis parallel to the loading axis (“ $c$  axial”), as measured in the longitudinal detector bank, there is a large compressive strain change during loading. This can be interpreted as lattice shrinkage along the  $c$  axis due to the domain switching. At around  $-150$  MPa applied stress, all the tetragonal domains that could align their  $c$  axis perpendicular to the applied load have done so leading to the saturation of axial strain. The remainders, still aligned so that they continue to contribute to the “ $c$  axial” data in the longitudinal detector, are pinned and can only deform elastically. The corresponding deformation in the transverse direction is captured by the “ $a$  trans.” strains in Fig. 5(a). Notice that they exhibit the expected Poisson effect and are positive. Since domain switching is mostly inactive during unloading, the axial strain cannot be relaxed, leaving a large negative residual strain of about  $-0.62\%$ , a measure of the depoling process. It is also interesting to note that the maximum value of the “ $c$  axial” strain (about  $0.8\%$ ) is close to the macroscopic axial strain measured by the strain gauge (Fig. 3). This suggests that the overall longitudinal strain of the specimen is largely determined by the domain switching process. On the other hand, domains that are aligned with their  $c$  axis perpendicular to the loading direction (and hence contribute to “ $a$  axial” and “ $c$  trans.”) experience mostly elastic loading and unloading. This is again expected since the orientation of these domains is already a low-energy configuration, leaving them with no driving force to switch under applied stress. As a result, they deform elastically.

### C. Rhombohedral phase

The rhombohedral phase is a minority phase in the specimens studied. Therefore, the results obtained from this phase should be viewed with caution, especially from the loaded specimen since the low counting statistics and the limited data resolution prevented a complete texture analysis as was discussed before. This is especially true for the transverse data due to the low coverage of the detector in that direction. However, the rhombohedral March coefficient ( $r_R$ ) in the longitudinal detector [Fig. 4(a)] is representative of the loaded specimen in the axial direction due to the superior sampling statistics of that detector. Initial values of  $r_R$  and  $r_T$  indicate that the rhombohedral phase of this PZT was more effectively poled electrically compared to the tetragonal phase [Fig. 4(a)]. As the load increased, a similar behavior is observed in the rhombohedral phase as was in the

tetragonal only more severe, indicating that in the mechanical depoling process too, this phase is more easily reoriented. March coefficient data from the transverse detector [Fig. 4(b)] were not very reliable in the low-load regime, but the trend and maxima confirm the switching observed in the longitudinal detector bank.

Figure 5(b) shows the lattice strain evolution in the rhombohedral phase. Here, the  $a$  and  $c$  axes correspond to the  $[1-10]$  and  $[111]$  directions in the pseudocubic unit cell, respectively. It is seen that both “ $a$  axial” and “ $c$  axial” display the expected compressive behavior, but for this phase the magnitudes are roughly the same, in contrast to the tetragonal phase. Similar to the tetragonal case, the maximum values of both strains are near the value measured by the strain gauge (Fig. 3). In the transverse bank where the sampling statistics are already hindered, the strain data allow only for the confirmation of a tensile strain trend due to the Poisson effect.

### D. Combined texture analysis

While the March function provides an accurate description of the texture in this material, it is also desirable to form a more quantitative picture of the domain switching. Following the formulation of Bedoya *et al.*, the fraction of domains switched both due to the initial electrical poling and subsequent mechanical depoling process may be calculated.<sup>5</sup> Defining the relative intensity ratios as

$$T = I(002)_T / [I(200)_T + I(002)_T], \quad (3)$$

$$R = I(006)_R / [I(202)_R + I(006)_R], \quad (4)$$

one may calculate the fraction of domains switched ( $\eta_T$  and  $\eta_R$ ), relative to a random orientation distribution and including intensity variations due to structure factor differences, as

$$\eta_T = \frac{T' - T}{2T + T' - 3T \cdot T'}, \quad (5)$$

$$\eta_R = \frac{R' - R}{3R + R' - 4R \cdot R'}, \quad (6)$$

where the prime signifies intensity ratios at a given load condition, and nonprime is the reference intensity ratio from the randomly oriented configuration. Observed, normalized intensities for individual peaks were extracted from the Rietveld analysis. All calculations were performed with respect to the powder sample, which was designated as having no preferred grain orientation, corresponding to “0 fraction of domains switched” (Fig. 6). By using the powder as a reference, the quantification of the effectiveness of both electrical poling and mechanical depoling was possible.

The results of these calculations for the longitudinal detector are plotted in Fig. 6. Positive values in this plot indicate the fraction of domains which have switched (relative to the random configuration) so that their unit cell dipoles are parallel to the sample axis. For the tetragonal phase only, the negative values correspond concisely to a fraction of domains switched (again relative to the random configuration) so that their  $c$  axes are perpendicular to the sample axis. In

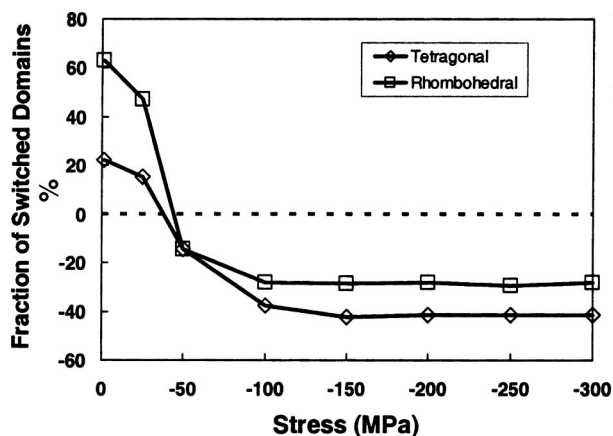


FIG. 6. Calculated fraction of switched domains in the loaded specimen with respect to the powder case. The data were extracted from the longitudinal detector.

the poled configuration at zero load the rhombohedral phase has 63% of its domains aligned with their dipole directions parallel to the sample axis, while the tetragonal has only 22%. The data for the rhombohedral phase are in good agreement with Bedoya *et al.*,<sup>5</sup> but the tetragonal phase exhibits only weak initial poling in comparison. Again it is evident that in our specimen the rhombohedral phase was more effectively poled using the electric field. As the load is increased the rhombohedral phase clearly responds more quickly than the tetragonal phase, though both phases pass through the zero point (the random configuration) between  $-25$  and  $-50$  MPa in agreement with the March coefficient data from this detector. Here too, the switching process is saturated by  $-150$  MPa in both phases, but the rhombohedral phase does not exhibit a higher amount of alignment in the normal direction than the tetragonal phase, as might be expected. The reason for this is that the negative fraction data for the rhombohedral phase is not as easy to interpret compared to the tetragonal phase. In the latter, the increase of the (200) intensity in the longitudinal data (leading to negative fraction values) means that more tetragonal domains have switched so that their  $c$  axis is in the transverse direction. In this case, it is worth noting that while only 22% of these domains were initially aligned along the sample axis (due to the electrical poling), around 40% were switched by the applied stress (Fig. 6). This result suggests that mechanical loading was more effective in this specimen than the electrical loading (or, alternatively, some relaxation occurred after the electrical poling). For the rhombohedral phase, in addition to the insufficient texture model described earlier (which could not consider the  $[202]$  pole), the domain switching is not orthogonal. The only certain conclusion for this phase is that the texture model sufficiently accounts for the changing intensities in the low-load region of Fig. 6, corresponding to the regime where the majority of the rhombohedral domains remain in the poled (not switched) position. After passing through the random configuration value of zero and into the negative fraction region of Fig. 6, the intensity of the (006) peak decreased only slightly with applied stress whereas that of the (202) was relatively constant because  $71^\circ$  or  $109^\circ$

switching does not move the  $[202]$  pole into a position where it satisfies the diffraction condition for the longitudinal detector. Thus the texture model in this range is insufficient to correctly supply data for Eqs. (4) and (6). While the effect of domain switching could be clearly observed, its exact quantification in the high-applied-stress regime is not possible with the current experimental setup and data.

## V. CONCLUSIONS

Neutron diffraction data were collected *in situ* on morphotropic, prepoled PZT samples under compressive loads. Structural analysis via Rietveld refinement showed significant texture present after the electrical poling procedure. Through application of the March–Dollase model, simultaneous bulk measurements of texture and lattice strains were possible in these materials. Most of the tetragonal phase experienced domain switching between  $-25$  and  $-150$  MPa, where the process saturated. As a result of this switching, highly anisotropic lattice strains were observed. Similar trends were seen in the minority rhombohedral phase, though data indicate that this phase responds more readily both to electric fields and applied stresses. Although only a relatively small amount of this phase was present in the material, the ease with which it responds to external stimuli and the large lattice strains observed in it confirm that this phase plays a significant role in the macroscopic electromechanical behavior of this material. Given the uncertainties in the analysis, we nonetheless draw the conclusions that the rhombohedral phase was more strongly oriented by the prior electric field poling than the tetragonal phase. On the other hand, the tetragonal phase was likely more strongly depoled by the mechanical loading than it was poled electrically.

The successful extraction of  $hkl$ -dependent strains (combined with the quantitative texture information) will allow for further verification and adaptation of the new self-consistent models for ferroelectrics.<sup>2</sup> In these models, different variants of domains are monitored as they switch (and convert into another) as a function of applied electromechanical loading. The interactions of variants and grains within a polycrystalline body determine the overall response of the material. The diffraction data obtained in this study can be used to compare model predictions with the material's actual response in different crystallographic directions allowing the calculation of important parameters such as critical switching stress and kinematic hardening coefficients.<sup>2</sup> This work is currently in progress.

## ACKNOWLEDGMENTS

This study is supported by the Multidisciplinary University Research Initiative at Caltech on Engineering Microstructural Complexity in Ferroelectric Devices (Army Research Office Grant No. DAAD19-01-1-0517) and the National Science Foundation (CAREER Grant No. DMR-9985264).

<sup>1</sup>J. M. Calderon-Moreno, Mater. Sci. Eng., A **315**, 227 (2001).

<sup>2</sup>J. E. Huber, N. A. Fleck, C. M. Landis, and R. M. McMeeking, J. Mech. Phys. Solids **47**, 1663 (1999).

<sup>3</sup>J. M. Calderon-Moreno, Key Eng. Mater. **206-213**, 1445 (2002).

- <sup>4</sup>S. C. Hwang, C. S. Lynch, and R. M. McMeeking, *Acta Metall. Mater.* **43**, 2073 (1995).
- <sup>5</sup>C. Bedoya, Ch. Muller, J.-L. Baudour, V. Madigou, M. Anne, and M. Roubin, *Mater. Sci. Eng., B* **75**, 43 (2000).
- <sup>6</sup>J. C. Fernandes, D. A. Hall, M. R. Cockburn, and G. N. Greaves, *Nucl. Instrum. Methods Phys. Res. B* **97**, 137 (1995).
- <sup>7</sup>A. Endriss, M. Hammer, M. J. Hoffmann, A. Kolleck, and G. A. Schneider, *J. Eur. Ceram. Soc.* **19**, 1229 (1999).
- <sup>8</sup>K. Tanaka, Y. Akiniwa, Y. Sakaida, and H. Kimachi, *JSME Int. J., Ser. A* **43**, 351 (2000).
- <sup>9</sup>T. Tsurumi, Y. Kumano, N. Ikeda, N. Ohashi, and O. Fukanaga, *Key Eng. Mater.* **157-158**, 73 (1999).
- <sup>10</sup>T. Ogawa and K. Nakamura, *Jpn. J. Appl. Phys., Part 1* **37**, 5241 (1998).
- <sup>11</sup>X. Li, W. Y. Shih, J. S. Vartuli, D. L. Milius, I. A. Aksay, and W. H. Shih, *J. Am. Ceram. Soc.* **85**, 844 (2002).
- <sup>12</sup>A. P. Wilkinson, J. Xu, S. Pattanaik, and S. J. L. Billinge, *Chem. Mater.* **10**, 3611 (1998).
- <sup>13</sup>J. Frantti, J. Lappalainen, S. Eriksson, V. Lantto, S. Nishio, M. Kakihana, S. Ivanov, and H. Rundlof, *Jpn. J. Appl. Phys., Part 1* **39**, 5697 (2000).
- <sup>14</sup>D. L. Corker, A. M. Glazer, R. W. Whatmore, A. Stallard, and F. Fauth, *J. Phys.: Condens. Matter* **10**, 6251 (1998).
- <sup>15</sup>A. M. Glazer and S. A. Mabud, *Acta Crystallogr., Sect. B: Struct. Crystallogr. Cryst. Chem.* **34**, 1065 (1978).
- <sup>16</sup>A. M. Glazer, S. A. Mabud, and R. Clark, *Acta Crystallogr., Sect. B: Struct. Crystallogr. Cryst. Chem.* **34**, 1060 (1978).
- <sup>17</sup>H. Horiuchi, T. Kobayashi, and A. J. Schultz, *Jpn. J. Appl. Phys., Part 1* **30**, 2035 (1991).
- <sup>18</sup>S. T. Misture, S. M. Pilgrim, J. C. Hicks, C. T. Blue, E. A. Payzant, and C. R. Hubbard, *Appl. Phys. Lett.* **72**, 1042 (1998).
- <sup>19</sup>B. Jaffe, W. R. Cook, and H. Jaffe, *Piezoelectric Ceramics* (Academic Press, New York, 1971).
- <sup>20</sup>M. A. M. Bourke, D. C. Dunand, and E. Üstündag, *Appl. Phys. A: Mater. Sci. Process.* **74**, S1707 (2002).
- <sup>21</sup>M. R. Daymond and H. G. Priesmeyer, *Acta Mater.* **50**, 1613 (2002).
- <sup>22</sup>H. M. Rietveld, *J. Appl. Crystallogr.* **2**, 65 (1969).
- <sup>23</sup>A. C. Larson and R. B. Von Dreele, *GSAS: General Structure Analysis System*, Los Alamos National Laboratory, Report No. LAUR 86-748, 1986.
- <sup>24</sup>Ch. Muller, J.-L. Baudour, C. Bedoya, F. Bouree, J.-L. Soubeyroux, and M. Roubin, *Acta Crystallogr., Sect. B: Struct. Sci.* **56**, 27 (2000).
- <sup>25</sup>C. Bedoya, Ch. Muller, J.-L. Baudour, F. Bouree, J.-L. Soubeyroux, and M. Roubin, *J. Phys.: Condens. Matter* **13**, 6453 (2001).
- <sup>26</sup>*The Rietveld Method*, edited by R. A. Young (Oxford University Press, Oxford, 1996), p. 22.
- <sup>27</sup>A. March, *Z. Kristallogr.* **81**, 285 (1932).
- <sup>28</sup>W. A. Dollase, *J. Appl. Crystallogr.* **19**, 267 (1986).
- <sup>29</sup>M. G. Cain, S. M. Bennington, M. H. Lewis, and S. Hull, *Philos. Mag. B* **69**, 499 (1994).
- <sup>30</sup>D. Berlincourt, *J. Acoust. Soc. Am.* **91**, 3034 (1992).